

Microrheology of semiflexible filament solutions based on relaxation simulations

L. K. R. Duarte, A. V. N. C. Teixeira, L. G. Rizzi

Departamento de Física, Universidade Federal do Viçosa, CEP 36570-000, Viçosa, MG, Brazil.

Abstract

We present an efficient computational methodology to obtain the full viscoelastic response of dilute solutions of unentangled semiflexible filaments. By considering an approach based on the fluctuation-dissipation theorem, we were able to evaluate the dynamical properties of long semiflexible filaments from relaxation simulations with a relatively low computational cost and higher precision in comparison to the traditional brownian dynamics simulations. We used a microrheological approach to obtain the complex shear modulus and the complex viscosity of the solution through its compliance which was obtained directly from the dynamical properties of the filaments. The relaxation simulations were applied to access the effects of the bending energy on the viscoelasticity of semiflexible filament solutions and our methodology was validated by comparing the numerical results to experimental data on DNA and collagen solutions.

Keywords:

semiflexible filaments, unentangled solutions, microrheology, relaxation simulations, fluctuation-dissipation theorem

1. Introduction

Despite of its importance to the well-functioning of almost all biological specimens [1], the viscoelastic response of complex solutions of unentangled semiflexible filaments [2], *e.g.*, collagen, actin, rodlike viruses, amyloid fibrils, microtubules, and DNA, is not yet entirely predictable neither from theory or simulations [3]. Contrary to solutions of cross-linked filaments, where a shear protocol can be used to extract the mechanical properties of the networks [4, 5, 6, 7], the study of the viscoelastic response of solutions of diluted unentangled filaments relies mainly on monitoring the stochastic dynamics of segments in the filament, which means that those methods are based mainly on fluctuations due to Brownian dynamics [8]. Alternatively, one could consider relaxation approaches which are based on fluctuation-dissipation theorem (FDT), just as done experimentally in the microrheological characterization of complex solutions [9, 10, 11]. However, even though computational simulations based on FDT have been used to obtain the dynamics of ideal polymer networks [12, 13, 14], such relaxation simulations have not been applied to obtain the viscoelastic properties of solutions; that is the focus of the present study.

The remainder of the paper is as follows. First, we review the relevant theoretical and computational aspects related to the rheology and microrheology of solutions of unentangled filaments. In Sec. 3 we describe a simple bead-spring filament model and present the numerical methods used to perform the simulations, including the technique based on relaxation simulations, which allow us to extract the viscoelastic properties of solutions from the dynamics of the beads in the filament. In Sec. 3 we also include a comparison between the results obtained from our simulations for flexible filaments and the usual Brownian dynamics simulations, as well as a comparison between our numerical results and the experimental data obtained for flexible polyelectrolytes. Our results for semiflexible filaments are presented in Sec. 4, where we investigate the effects of bending on the viscoelasticity of diluted solutions and we also include comparisons between our numerical results and experimental data obtained for DNA and collagen macromolecules. In the last section we present our concluding remarks and indicate how the method can be useful to simulations that incorporate more detailed models of semiflexible filaments.

Email address: lerizzi@ufv.br (L. G. Rizzi)

2. Viscoelasticity of unentangled solutions

Experimentally, one can characterize the mechanical properties of viscoelastic fluids by considering, *e.g.*, steady-state shearing experiments [15], where the time-dependent stress $\sigma(t)$ of the viscoelastic material is related to its relaxation modulus $G(\tau)$ as [16, 17]

$$\sigma(t) = \int_{-\infty}^t dt' G(t-t') \dot{\gamma}(t') , \quad (1)$$

with $\dot{\gamma}$ being the shear rate. Also, one can consider small-amplitude oscillatory shearing experiments [15] with $\gamma(t)$ being an oscillatory function so that the viscoelastic response of the fluid is given by the complex shear modulus, $G^*(\omega) = G'(\omega) + iG''(\omega)$, where $G'(\omega)$ and $G''(\omega)$ correspond to the storage and the loss modulus, respectively. At the linear viscoelastic (LVE) response regime, both experimental techniques should provide the same information, as the complex modulus is directly related to $G(\tau)$ via a Fourier transform [15, 18], that is,

$$G^*(\omega) = i\omega \int_0^{\infty} d\tau' G(\tau') e^{-i\omega\tau'} . \quad (2)$$

For viscoelastic solutions, it is also convenient to obtain the complex viscosity [15], $\eta^*(\omega) = \eta'(\omega) - i\eta''(\omega)$, which is related to the complex modulus as $G^*(\omega) = i\omega\eta^*(\omega)$, so that $\eta'(\omega) = G''(\omega)/\omega$ and $\eta'' = G'(\omega)/\omega$. At low frequencies, the loss modulus of viscoelastic solutions is expected to be proportional to the frequency, *i.e.*, $G''(\omega) \propto \omega$, so the viscosity $\eta'(\omega)$ should be independent of the frequency and is related to the relaxation modulus as [18]

$$\eta_0 = \lim_{\omega \rightarrow 0} \eta'(\omega) = \int_0^{\infty} d\tau' G(\tau') , \quad (3)$$

which is equivalent to the steady-state viscosity $\eta(\dot{\gamma}) = \sigma(\dot{\gamma})/\dot{\gamma}$ that is obtained for low shear rates at the LVE regime [19].

Alternatively, the viscoelasticity of complex solutions can be obtained by microrheological techniques [20, 21], which are based on relationships between the viscoelastic response of the material and the dynamics of probe particles immersed on it (see, *e.g.*, Ref. [22]). In particular, one can explore passive experimental approaches (*e.g.*, particle tracking videomicroscopy or dynamic light scattering; see Ref. [1] for a review) to extract the mean-squared displacement (MSD) $\langle \Delta r^2(\tau) \rangle_a$ of probe particles with radius a and relate it to the compliance $J(\tau)$ of the so-

lution through a generalized Stokes-Einstein relationship [20, 23], that is,

$$J(\tau) = \frac{3\pi a}{dk_B T} \langle \Delta r^2(\tau) \rangle_a , \quad (4)$$

where d is the euclidean dimension of the random walk, k_B is the Boltzmann's constant, and T is the absolute temperature of the medium.

At the LVE regime, microrheology and rheology should give the same information about the viscoelastic behaviour of the solution. This because the relaxation modulus is linked to the compliance $J(\tau)$ of the solution through a convolution [16],

$$\int_0^{\tau} G(\tau - \tau') J(\tau') d\tau' = \tau , \quad (5)$$

and one can evaluate the complex shear modulus directly from the Fourier transform of the compliance $\hat{J}(\omega)$ as

$$G^*(\omega) = \frac{1}{i\omega \hat{J}(\omega)} . \quad (6)$$

Just like it is done for polymeric solutions [24], one can assume that, at low concentrations of filaments, the effect of the presence of filaments on the relaxation modulus of the solution is additive, so that

$$G(\tau) = n_{\phi} G_f(\tau) , \quad (7)$$

where $G_f(\tau)$ corresponds to the relaxation modulus of an isolated filament and n_{ϕ} is a dimensionless number that should be proportional to the volume fraction ϕ (or the mass concentration c) of filaments in solution. Also, by inserting Eq. (7) into Eq. (3) one finds that the same additive contribution due to the presence of filaments takes place in the viscosity of the solution, and one can estimate the viscosity due to an isolated filament as

$$\eta_{0,f} = \frac{\eta_0}{n_{\phi}} . \quad (8)$$

Since the compliance of the solution is given by $J(\tau) = \tau/\eta_0$ at time intervals τ longer than the longest relaxation time of the filament τ_f , one can also infer that the compliance of the solution should be given as

$$J(\tau) = \frac{J_f(\tau)}{n_{\phi}} , \quad (9)$$

where $J_f(\tau)$ correspond to the compliance due to an isolated filament, that is,

$$J_f(\tau) = \frac{1}{2dD_f\eta_{0,f}} \langle \Delta r^2(\tau) \rangle_f . \quad (10)$$

with $\langle \Delta r^2(\tau) \rangle_f$ and D_f being the MSD and the diffusion coefficient of center of mass of the filament, respectively. Indeed, by considering Eqs. (7) and (9), one can verify that the convolution between the relaxation modulus $G_f(\tau)$ and the compliance $J_f(\tau)$ of isolated filaments, is equivalent to the convolution between $G(\tau)$ and $J(\tau)$ given by Eq. (5). The above equations indicate that, while an increase in the concentration of filaments lead to a increase in n_ϕ , hence in $G(\tau)$ and η_0 , it should decrease the compliance $J(\tau)$ of the solution. Clearly, Eqs. (7), (8), and (9) are expected to be valid only for highly diluted solutions (*i.e.*, for $n_\phi \rightarrow 0$), similarly to what is often done to evaluate the intrinsic viscosities and the reduced relaxation moduli of polymeric solutions [24].

Finally, by considering that the filament can be described by a chain with N segments, one can estimate the relaxation modulus of the solution $G(\tau)$ directly from the dynamics of a single segment, *i.e.*, a Kuhn segment. This because the diffusion of a segment should be limited by the diffusion of the whole filament and one can verify that, at long time intervals, the MSD of the segment's position, $\langle \Delta r^2(\tau) \rangle_s$, should coincide with the MSD of the center of mass of the filament, $\langle \Delta r^2(\tau) \rangle_f$, so that it can be replaced into Eq. (10). Hence, Eqs. (6), (9), and (10) establish a direct link between the stochastic dynamics of the segments in the filament and the complex shear modulus of the solution. Indeed, as it can be verified for flexible polymers described by the Rouse model [24], if the MSD of the segments display a characteristic subdiffusive behaviour, that is, $\langle \Delta r^2(\tau) \rangle_s \propto \tau^\alpha$ with $\alpha < 1$, then the shear moduli will present a power-law behaviour with the same exponent, that is, $G'(\omega) \propto G''(\omega) \propto \omega^\alpha$ (for Rouse chains $\alpha = 1/2$).

For semiflexible chains, in particular, recent molecular dynamics simulations [25] indicate that the MSD of Kuhn segments display an exponent $\alpha = 3/4$, which agreed with several theoretical approaches [17, 26], and experimental evidence [3, 27, 28, 29] presented in the literature. Interestingly, Ref. [25] confirmed results obtained in Refs. [30, 31, 32] that both bond autocorrelation and end-to-end vector correlation functions (which are extracted from an isolated chain and can be related to the relaxation modulus), display a power-law behaviour that lead to a similar exponent.

3. Methods

In this section we describe the filament model and the numerical procedures to obtain the dynamical properties of the filaments, as well as the shear moduli and the complex viscosity of the solution.

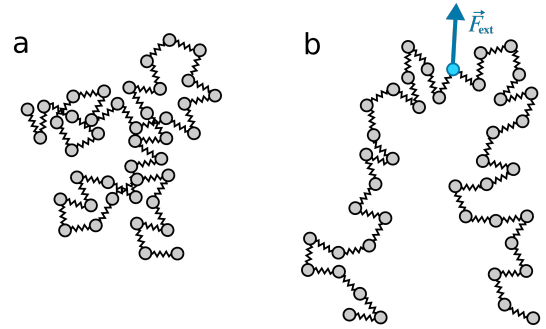


Figure 1: Bead-spring model that is used to represent both flexible and semiflexible filaments. The separation between beads depends on their interactions, which are determined by the spring (κ) and bending (κ_b) constants defined in Eqs. (11) and (12), respectively, and also on the friction coefficient ζ between the beads and the solvent, which is given in terms of the diffusion coefficient D_0 , as in Eq. (16). (a) denote a configuration of the filament in the overdamped Langevin approach, where the dynamics is due to Brownian motion. (b) illustrate the relaxation approach, where an external force \vec{F}_{ext} is used to pull the m -th bead in the middle of the filament.

3.1. Filament model

As illustrated in Fig. 1, the semiflexible filaments are modelled by a simple bead-spring model with N beads in a implicit solvent with viscosity η_s at a temperature T . The beads are coupled to their nearest neighbours by an interaction potential that includes contributions from both harmonic (U_h) and bending (U_b) energies.

The harmonic interaction potential of the whole filament can be written as

$$U_h = \frac{\kappa}{2} \sum_{j=1}^{N-1} (\vec{r}_{j+1} - \vec{r}_j)^2, \quad (11)$$

where \vec{r}_j is the position vector of the j -th bead and κ is the effective spring constant. One can relate pre-factor in Eq. (11) to the pre-factor of the Gaussian chain model [24], so that $\kappa = 3k_B T / b^2$, where b is a parameter that sets the length scale (*e.g.*, nm) and the strength of the harmonic interaction in our simulations.

For the bending interaction potential we assume its discretized approximation (see, *e.g.*, [33]), which is evaluated as the sum of local curvatures along the filament and is given by

$$U_b = \frac{\kappa_b}{2} \sum_{j=2}^{N-1} (\vec{r}_{j-1} - 2\vec{r}_j + \vec{r}_{j+1})^2, \quad (12)$$

where $\kappa_b = E/b^4$ is the bending constant, with E being a parameter that sets the bending stiffness. Both constants κ and κ_b are given in units of force per length,

e.g., pN/nm. The value of κ_b can be approximately related to the persistent length of the filament as L_p , since it should be proportional to $A \equiv E'/b$, with $E' = E/k_B T$ (e.g., if E is given in pN.nm³ and b in nm, E' is given in nm², and L_p and A in nm).

3.2. Overdamped dynamics

In order to validate our approach, we first obtain the dynamical properties of the filament by implementing Brownian dynamics simulations, which consist in solving numerically the overdamped Langevin equation. For the i -th bead in the filament, such equation can be written as

$$\frac{\partial \vec{r}_i}{\partial t} = \frac{1}{\zeta} (\vec{F}_i + \vec{f}_a) , \quad (13)$$

where \vec{f}_a is a random force due to interaction of the bead with the implicit solvent, ζ is a time-independent friction coefficient, and \vec{F}_i is the total force exerted on the i -th bead which is determined from the interaction potentials defined by Eqs. (11) and (12), i.e., $\vec{F}_i = -\nabla_i(U_h + U_b)$, with $\nabla_i = \partial_{x_i}\hat{x} + \partial_{y_i}\hat{y} + \partial_{z_i}\hat{z}$.

Note that one can assume either free boundary conditions (FBC) or periodic boundary conditions (PBC). In the case of PBC, one can consider the displacement vectors between consecutive beads, $\vec{r}_j = \vec{r}_{j+1} - \vec{r}_j$, in order to accommodate the correct indexing in Eqs. (11) and (12) at the filament's ends, that is, $\vec{r}_0 = \vec{r}_1 - \vec{r}_{N-1}$ and $\vec{r}_{-1} = \vec{r}_0 - \vec{r}_{N-2}$, and also, $\vec{r}_{N+1} = \vec{r}_N + \vec{r}_1$ and $\vec{r}_{N+2} = \vec{r}_{N+1} + \vec{r}_2$.

In practice, one has $3N$ coupled differential equations defined as in Eq. (13), which are discretized and solved numerically by considering the Euler integration scheme, so that the position vector of the i -th bead at a time $t + \Delta t$ is given by

$$\vec{r}_i(t + \Delta t) = \vec{r}_i(t) + \frac{\Delta t}{\zeta} (\vec{F}_i + \vec{f}_a) , \quad (14)$$

where the k -th component of the random force is evaluated as [34]

$$f_{a,k} = \sqrt{\frac{2\zeta k_B T}{\Delta t}} N_k(0, 1) , \quad (15)$$

with $N_k(0, 1)$ (for $k = x, y, \text{ or } z$) a random variable obtained from a gaussian distribution with zero mean and variance equal to one. The value of ζ is determined by the Stokes-Einstein relation, that is,

$$\zeta = \frac{k_B T}{D_0} , \quad (16)$$

where D_0 defines the diffusion coefficient of a non-connected bead.

As discussed in Sec. 2, the dynamics of the filaments can be characterized by the fluctuations in the position of its segments, here denoted by its beads, which is quantified by their mean-squared displacement,

$$\langle \Delta r^2(\tau) \rangle = \langle [\vec{r}(\tau + t_0) - \vec{r}(t_0)]^2 \rangle , \quad (17)$$

where $\langle \dots \rangle$ denote averages over both N_T beads and M realizations of the numerical experiment. The initial configuration in each numerical simulation corresponds to a fully stretched filament with the beads separated by a distance b , and the averages are taken only after a thermalization period of time t_0 .

The time-dependent diffusion coefficient $D(\tau)$ of the segments can be retrieved from the time derivative of the MSD of the bead's position, that is

$$D(\tau) = \frac{1}{2d} \frac{\partial \langle \Delta r^2(\tau) \rangle}{\partial \tau} . \quad (18)$$

For all simulations we consider that the euclidean dimension is $d = 3$. It is worth mentioning that, in order to avoid boundary effects on $\langle \Delta r^2(\tau) \rangle$ and $D(\tau)$ when using FBC, we consider that the average is taken over the $N_T = N - 2N_E$ beads which are centrally localized in the filament, i.e., excluding N_E beads on each side. In the case of PBC we simply consider $N_T = N$.

Figure 2 shows the MSD and the diffusion coefficient obtained for a flexible filament, i.e., without bending energy, just to validate our approach. Such flexible filament can be well described by the Rouse model [17, 24] and, as expected, the MSD displays two normal diffusion regimes: one for times shorter than $\tau_0 = k_B T / (\pi^2 \kappa D_0)$, with $\langle \Delta r^2(\tau) \rangle = 6D_0\tau$, which corresponds to the free-like displacements of the beads; and the other for times longer than $\tau_R = \tau_0 N^2$, with $\langle \Delta r^2(\tau) \rangle = 6(D_0/N)\tau$, which corresponds to the diffusion of the centre of mass of the filament. Also, the Rouse model displays an intermediate regime with a characteristic subdiffusive anomalous behaviour [24], where $\langle \Delta r^2(\tau) \rangle = \sqrt{36k_B T D_0 / (\pi \kappa)} \tau^{1/2}$. As shown in Fig. 2(b), those regimes are better identified by the time-dependent diffusion coefficient $D(\tau)$, which shows a transient power-law regime, i.e., $D(\tau) = \sqrt{k_B T D_0 / (4\pi \kappa)} \tau^{-1/2}$, between two plateaus, one with $D(\tau) = D_0$ at times shorter than $\tau_0 = 0.0034$ ms, and the other with $D(\tau) = D_R = D_0/N$, at times longer than $\tau_R = 34$ ms (here we have considered $N = 100$, $D_0 = 90$ nm²/ms, $k_B T = 4.142$ pN.nm, $\kappa = 1.38$ pN/nm, and $\kappa_b = 0$ pN/nm.).

Figure 2 also includes the comparison between the overdamped dynamics approach with the relaxation approach, which is described below.

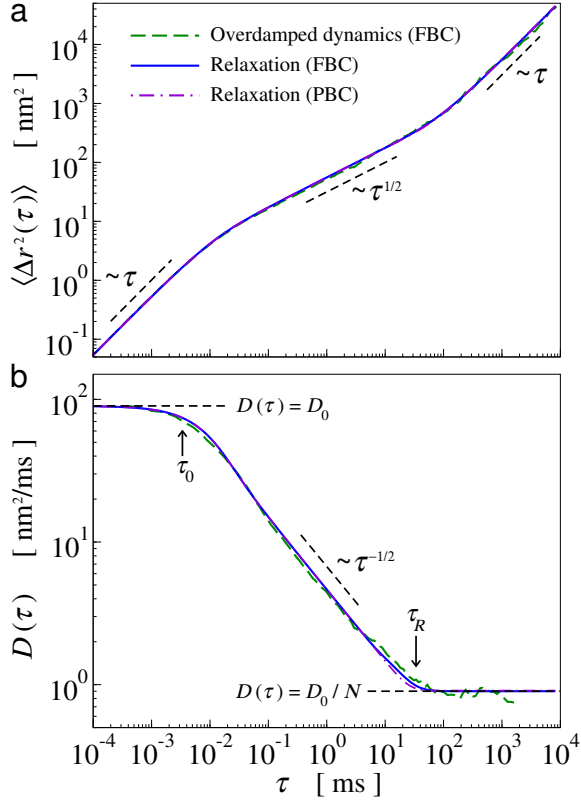


Figure 2: (a) Mean-squared displacement $\langle \Delta r^2(\tau) \rangle$, and (b) the time-dependent diffusion coefficient $D(\tau)$ as function of time τ , for a flexible filament (*i.e.*, no bending energy, $\kappa_b = 0$ pN/nm). Long-dashed green lines correspond to overdamped simulations with free boundary conditions (FBC), while dashed-dotted blue and straight purple lines correspond to relaxation simulations with (PBC) and without (FBC) periodic boundary conditions, respectively. Short-dashed black lines indicate the two normal diffusive behaviours where $\langle \Delta r^2(\tau) \rangle \propto \tau$ and $D(\tau)$ is constant, and the intermediary subdiffusive behaviour with $\langle \Delta r^2(\tau) \rangle \propto \tau^{1/2}$ and $D(\tau) \propto \tau^{-1/2}$, as expected from Rouse dynamics [24] (see text for details). For both numerical approaches the results were obtained with $N = 100$ beads, $D_0 = 90$ nm²/ms, $k_B T = 4.142$ pN.nm ($T = 300$ K), $b = 3$ nm, so that $\kappa = 1.38$ pN/nm, $\tau_R = k_B T N^2 / (\pi^2 \kappa D_0) \approx 34$ ms, and ζ is given by Eq. (16). For the overdamped simulations, the results correspond to average values obtained from $M = 100$ realizations with $N_E = 7$ after a thermalization of $t_0 = 5 \times 10^3$ ms (*i.e.*, 5×10^6 steps with $\Delta t = 10^{-3}$ ms). For the relaxation simulations no thermalization was required and we use a constant external force $F_0 = 1$ pN with the same Δt .

3.3. Relaxation approach based on FDT

In the relaxation approach, the MSD $\langle \Delta r^2(\tau) \rangle$ and the time-dependent diffusion coefficient $D(\tau)$ of the beads in the filament are evaluated from a relation that comes from the fluctuation-dissipation theorem (FDT) [18, 24].

Importantly, the use of the relaxation simulations based on FDT is restricted to the linear response regime which means that the intensity of the external force is

relatively weak but large enough so that one can neglect the random thermal forces \vec{f}_a . In this case one can solve the $3N$ coupled differential equations by using a Euler integration scheme similar to Eq. (19), but assuming that \vec{f}_a are close to zero, so that

$$\vec{r}_i(t + \Delta t) = \vec{r}_i(t) + \frac{\Delta t}{\zeta} \left(\vec{F}_i + \delta_{im} \vec{F}_{\text{ext}} \right), \quad (19)$$

where the Kronecker delta δ_{im} indicates that the constant external force $\vec{F}_{\text{ext}} = F_0 \hat{z}$ is applied only to the m -th bead in the middle of the filament, as illustrated in Fig. 1(b).

In practice, FDT can be used to link the displacement $\Delta z(\tau)$ of the m -th bead driven by the external force to the fluctuations on its position at equilibrium as [18]

$$\Delta z(\tau) = [z_m(\tau) - z_m(0)] = \chi_{zz}(\tau) F_0, \quad (20)$$

where $\chi_{zz}(\tau)$ is a linear response function given by

$$\chi_{zz}(\tau) = \frac{1}{2k_B T} \langle \Delta z^2(\tau) \rangle. \quad (21)$$

Hence, one can estimate the MSD of the beads in d dimensions as

$$\langle \Delta r^2(\tau) \rangle = \frac{2dk_B T}{F_0} [z_m(\tau) - z_m(0)]^2. \quad (22)$$

Also, one can retrieve the time-dependent diffusion coefficient $D(\tau)$ by derivating Eq. (22) just as prescribed by Eq. (18), which yields

$$D(\tau) = \frac{k_B T}{F_0} v_{m,z}(\tau), \quad (23)$$

where $v_{m,z}(\tau)$ is the velocity of the m -th bead, which can be directly obtained from the numerical integration scheme.

As one can see in Fig. 2, the results obtained from the relaxation approach with Eqs. (22) and (23) display a good agreement to those obtained from usual overdamped simulations. It is worth mentioning that, since one does not have to compute averages over M realizations and it does not require the thermalization step (*i.e.*, the initial configuration corresponds to a fully stretched filament placed along a direction that is perpendicular to z with a separation b between beads), the numerical approach based on relaxation dynamics is far more efficient than the one based on overdamped dynamics. For instance, the results obtained from relaxation simulations presented in Fig. 2 took less than a minute to be produced, while the simulations using overdamped dynamics required several hours. Also, the

numerical data obtained from relaxation simulations is not noisy as those obtained from the overdamped simulations. That is very convenient since, as we discuss in the following, one have to compute Fourier transforms of $\langle \Delta r^2(\tau) \rangle$ in order to extract the viscoelastic properties of the solutions.

3.4. Viscoelastic properties

As discussed in Sec. 2, the viscoelastic properties of the filament solution are characterized by the complex shear modulus $G^*(\omega) = G'(\omega) + iG''(\omega)$, which can be evaluated from the Fourier transform of the compliance of the solution $J(\tau)$ through Eq. (6).

Equation (9) provide a way to evaluate the compliance of the solution $J(\tau)$ in terms of the compliance $J_f(\tau)$ of an ultra-diluted solution, which, in turn, can be computed via Eq. (10) from the MSD of the center of mass of the filament $\langle \Delta r^2(\tau) \rangle_f$ and the long time diffusion coefficient D_f . Since the dynamics of both beads and filament are equivalent at long times, the time-independent diffusion coefficient of the filament D_f can be estimated directly from time-dependent diffusion coefficient $D(\tau)$ of the beads as

$$D_f = \lim_{\tau \rightarrow \infty} D(\tau) . \quad (24)$$

As mentioned in Sec. 2, the dynamics of the center of mass of the filaments should coincide with the dynamics of beads, *i.e.*, $\langle \Delta r^2(\tau) \rangle_f = \langle \Delta r^2(\tau) \rangle$, thus one can use Eqs. (9) and (10) to evaluate the compliance of the whole solution as

$$J(\tau) = \frac{1}{2dD_f\eta_0} \langle \Delta r^2(\tau) \rangle . \quad (25)$$

By assuming that the diffusion coefficient of an isolated filament can be estimated as

$$D_f \approx \frac{a_f^2}{2d\tau_f} \approx \frac{k_B T}{6\pi a_f \eta_{0,f}} , \quad (26)$$

where a_f is a characteristic length that might be interpreted as an effective radius of the filament, and τ_f is the longest relaxation time of the filament, one can use Eq. (8) to estimate the viscosity of the solution (at the low frequency limit) as

$$\eta_0 \approx n_\phi \frac{2d k_B T \tau_f}{6\pi a_f^3} \approx \frac{4}{3} n_f k_B T \tau_f , \quad (27)$$

where $n_f = \phi/V_f$ is the number density of filaments in solution, with $\phi \approx n_\phi$ being the volume fraction of filaments and $V_f \approx 4\pi a_f^3/3$ the effective volume of

the filament. Although we assume that the filaments have spherical shapes to obtain the above expression, Eq. (27) can be considered a somewhat general expression, as indicated by similar theoretical results obtained for different polymer models [17, 18].

Finally, by considering that the viscosity of the solution is approximately given by Eq. (27), its compliance can be estimated by Eq. (25), which can be rewritten as

$$J(\tau) = \frac{3}{8d k_B T D_f \tau_f} \frac{\langle \Delta r^2(\tau) \rangle}{n_f} . \quad (28)$$

Evidently, except from n_f , all the other quantities can be directly extracted from the dynamics of the beads, as illustrated in Fig. 2 (for the Rouse model one have that $D_f = D_R$ and $\tau_f = \tau_R$).

In order to validate our approach, we include in Fig. 3 a comparison between the results obtained from our relaxation simulations and the experimental data presented in Ref. [10] on a solution of polyacrylamide (PAM) chains, which can be considered flexible polyelectrolyte chains. By realizing that, at high frequencies, the viscosity should be given approximately by $\eta'(\omega) \cong \eta_0/N$, with η_0 given by Eq. (27), one might use the experimental data to estimate the number of segments that should be used to describe the filament. In addition, by considering that, for flexible chains, the longest time of the filament should be given by the Rouse relaxation time [24], that is,

$$\tau_f \cong \frac{k_B T}{\pi^2 \kappa D_0} N^2 , \quad (29)$$

one can, in principle, estimate the values of κ and D_0 as well. For instance, since the experiments in Ref. [10] were done at $T = 25^\circ\text{C}$ (*i.e.*, $k_B T = 4.114$ pN.nm), one might assume $\kappa = 12.342$ pN/nm (with $b = 1$ nm) and $D_0 = 1$ nm²/s, which yields $\tau_f \cong 3.4$ s and $\tau_0 = \tau_f/N^2 \cong 0.034$ s. Thus, by considering the number density $n_f = 2.5 \times 10^{13}$ cm⁻³, we were able to find a good agreement between the compliance $J(\tau)$ obtained from our relaxation simulations and the experimental data, as shown in Fig. 3(a). Here we recall that the concentration of filaments w_f (given in % w/w) is related to the number density as

$$w_f = \frac{n_f M_f}{n_s M_s + n_f M_f} , \quad (30)$$

where M_f is the molecular weight of the filament, and n_s and M_s are the number density and molecular weight of the solvent molecules, respectively. Hence, by considering that the molecular weight of PAM chains is $M_{\text{PAM}} = 18 \times 10^6$ g/mol (see Ref. [10]), the number density and

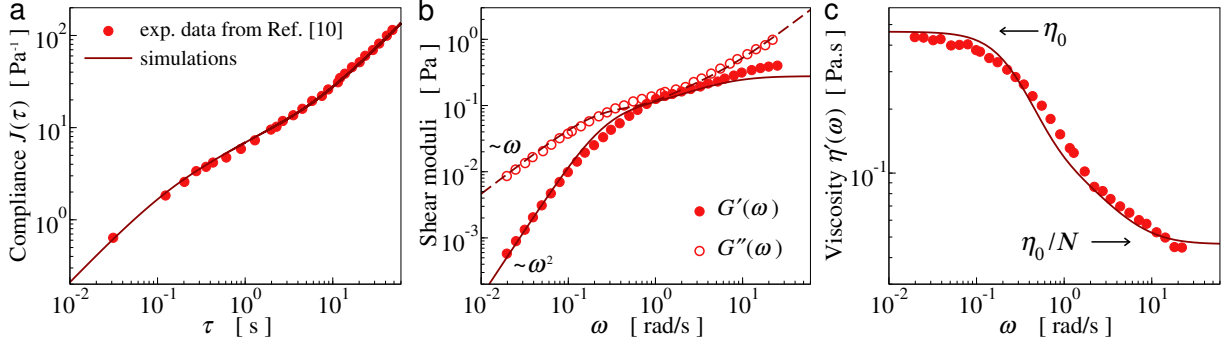


Figure 3: Comparison between the experimental data (circles) on flexible polyelectrolyte chains extracted from Ref. [10] and the numerical results obtained from the relaxation simulations (continuous lines). (a) Compliance $J(\tau)$, (b) storage modulus $G'(\omega)$ (filled circles) and loss modulus $G''(\omega)$ (open circles), and (c) viscosity $\eta'(\omega)$. Numerical estimates for the MSD of the beads $\langle \Delta r^2(\tau) \rangle$ were obtained via Eq. (22) from relaxation simulations implemented with PBC and using an external force equal to $F_0 = 1$ pN, $N = 10$ beads, $D_0 = 1$ nm²/s, $k_B T = 4.114$ pN.nm ($T = 298$ K), $b = 1$ nm, $\kappa = 12.342$ pN/nm, $\kappa_b = 0$ pN/nm (*i.e.*, flexible chains), and $\Delta t = 10^{-4}$ s. The match between the compliance $J(\tau)$ obtained from our numerical simulations through Eq. (28) and the experimental data of Ref. [10] was done by choosing a number density equal to $n_f = 2.5 \times 10^{13}$ cm⁻³, which is close to the number density n_{PAM} obtained from the nominal concentration of 0.07% w/w used in the experiments (see text for details). The complex shear modulus, $G^*(\omega)$, and the viscosity, $\eta'(\omega) = G''(\omega)/\omega$, were obtained from $J(\tau)$ via Eq. (6) using the numerical method proposed in Ref. [35].

the molecular weight of water molecules are, respectively, $n_{\text{water}} = 3.34 \times 10^{22}$ cm⁻³ and $M_{\text{water}} = 18$ g/mol, and that the concentration used in the experiments [10] was $w_{\text{PAM}} = 0.07\%$ w/w, one finds that the number density of PAM chains is $n_{\text{PAM}} \approx 2.33 \times 10^{13}$ cm⁻³, which is in good agreement with the value n_f used in Eq. (28) to obtain $J(\tau)$ from the MSD of the beads.

Now we consider Eq. (6) to obtain the complex shear modulus $G^*(\omega)$ from $J(\tau)$, where the Fourier transform of the compliance $\hat{J}(\omega)$ is evaluated numerically by the method proposed in Ref. [35] (see Ref. [27] for further details). In addition, we evaluate the complex viscosity from $G^*(\omega)$ as

$$\eta^*(\omega) = \frac{G^*(\omega)}{i\omega} . \quad (31)$$

Figures 3(b) and 3(c) indicates that both the storage $G'(\omega)$ and loss $G''(\omega)$ modulus, as well as the viscosity $\eta'(\omega) = G''(\omega)/\omega$, present a good agreement to the experimental data obtained from flexible chains [10]. In particular, Fig. 3(b) shows that, at low frequencies, $\omega \ll \tau_f^{-1} \approx 0.3$ rad/s, $G'(\omega) \propto \omega^2$ and $G''(\omega) \propto \omega$, which means that the viscosity $\eta'(\omega) = G''(\omega)/\omega$ goes to a constant value $\eta_0 \approx 0.47$ Pa.s, which agrees with the value computed from Eq. (27). As shown in Fig. 3(c), $\eta'(\omega)$ tends to a value η_0/N at high frequencies, thus, as mentioned earlier, one can consider those values to estimate the number of segments N of the filament to be used in the simulations.

4. Results

In the following we present numerical results obtained for semiflexible chains. In particular, we analyse the effect of bending energies on the dynamics of long filaments, demonstrating the effectiveness of our simulations based on the relaxation methodology described in Sec. 3.3.

Figure 4 include results obtained for semiflexible filaments composed by $N = 1000$ beads defined with different values for the bending constant κ_b but with a fixed spring constant κ . The results for the MSD and the time-dependent diffusion coefficient in Fig. 4 were obtained from relaxation simulations through Eqs. (22) and (23) with an external force equal to $F_0 = 1$ pN, $D_0 = 1$ nm²/ms, $k_B T = 4.142$ pN.nm ($T = 300$ K), $b = 1$ nm, $\Delta t = 10^{-6}$ ms, so that $\kappa = 12.426$ pN/nm and ζ given by Eq. (16). Importantly, we labelled the results in terms of $A \equiv E'/b$, which is a quantity that is directly related to the bending constant, as $\kappa_b = E/b^4$ and $E' = E/k_B T$ (see Sec. 3.1), and also because the persistent length L_p of the filaments should be proportional to A . In practice, higher values of κ_b correspond to greater values of A , and those can be interpreted as filaments with longer persistent lengths L_p .

Figures 4(a) and 4(b) show that the bending energy lead to significant changes in the dynamics of the beads. In particular, the short-time diffusion dynamics observed for flexible chains is altered to an extended subdiffusive regime where $\langle \Delta r^2(\tau) \rangle \propto \tau^\alpha$, with α approaching 3/4 as the value of A increases. This behaviour is confirmed in Fig. 4(b) by the time-dependent

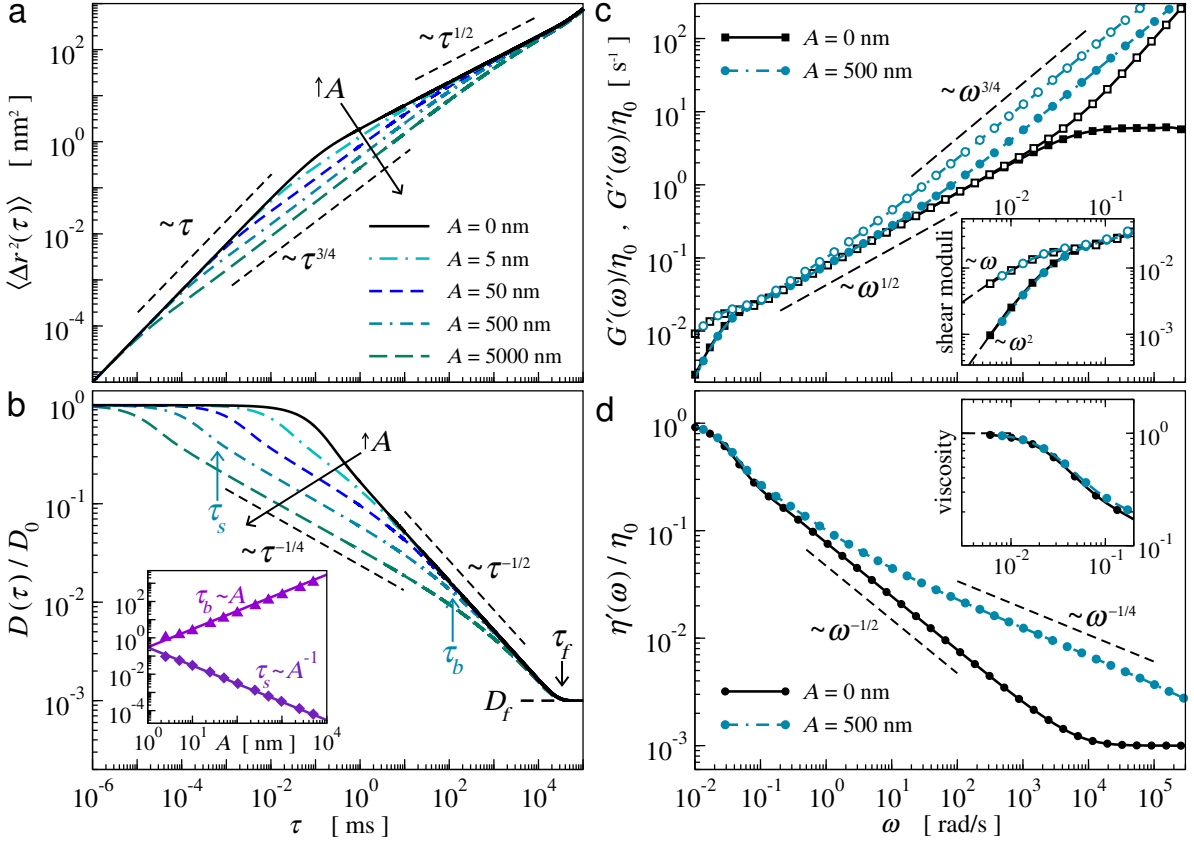


Figure 4: Effect of bending energies on the dynamics of semiflexible filaments and the viscoelastic properties of their corresponding solutions. Here we labelled the data in terms of $A = E'/b$, which should be proportional to both the bending constant $\kappa_b = E'k_B T/b^4$ and the persistent length L_p of the filaments. (a) Mean-squared displacement of the m -th bead $\langle \Delta r^2(\tau) \rangle$, Eq. (22); (b) time-dependent diffusion coefficient $D(\tau)$, Eq. (23) (Inset: characteristic times τ_s and τ_b as a function of A); (c) normalized storage modulus $G'(\omega)/\eta_0$ (filled symbols), and loss modulus $G''(\omega)/\eta_0$ (open symbols), obtained from the compliance $J(\tau)$, Eq. (25), through Eq. (6); and (d) normalized viscosity, $\eta'(\omega)/\eta_0$, Eq. (31). Inset panels of (c) and (d) are just zoomed in regions to show the low frequency regime. Results were obtained for long filaments with $N = 1000$ and different values of the bending constant κ_b from relaxation simulations with PBC and considering a constant external force $F_0 = 1$ pN, with $D_0 = 1$ nm²/ms, $b = 1$ nm, $k_B T = 4.142$ pN.nm ($T = 300$ K), $\Delta t = 10^{-6}$ ms, with a fixed spring constant $\kappa = 12.426$ pN/nm, and ζ given by Eq. (16). Short-dashed (black) lines indicate power-law behaviours observed for the dynamical and rheological quantities at different times.

diffusion coefficient $D(\tau)$, from where one can verify that the shortest relaxation time decreases as A (and κ_b) increases, while changes in the bending constant κ_b seems to not alter the longest relaxation time τ_f (at least for $A < 5000$ nm). Figure 4(b) indicate that higher values of A lead to a wider range of subdiffusive anomalous behaviour where $D(\tau) \propto \tau^{-1/4}$. By considering a local power-law approximation for the time-dependent diffusion coefficient, *i.e.*, $D(\tau) \propto \tau^\nu$, we computed the numerical derivatives of ν and, from its inflexion points, we determine two characteristic time scales, τ_s and τ_b , which comprise the range of subdiffusive behaviour that is directly related to the introduction of the bending energy, as illustrated for $A = 500$ nm in Fig. 4(b). Interestingly, our results indicate that both characteristic times

depend on A in a simple way and, as shown in the inset of Fig. 4(b), $\tau_s \approx 0.3 A^{-1}$ and $\tau_b \approx 0.3 A$. In addition, we observe that, at least for that range of A , the long time diffusion coefficient $D_f = D_0/N$ and the longest relaxation time τ_f remained unaltered, thus they can be conveniently evaluated from Rouse estimates through Eqs. (24) and (29), respectively.

As shown in Figs. 4(c) and 4(d), the changes in the short time dynamics of the segments clearly modify the high frequency viscoelastic response of the solution. In contrast to flexible chains, which display a characteristic exponent $\alpha = 1/2$ at high frequencies (see Ref. [24]), greater values of A lead to a subdiffusive anomalous behaviour so that the reduced moduli are given by $G'(\omega)/\eta_0 \propto \omega^\alpha$ and $G''(\omega)/\eta_0 \propto \omega^\alpha$,

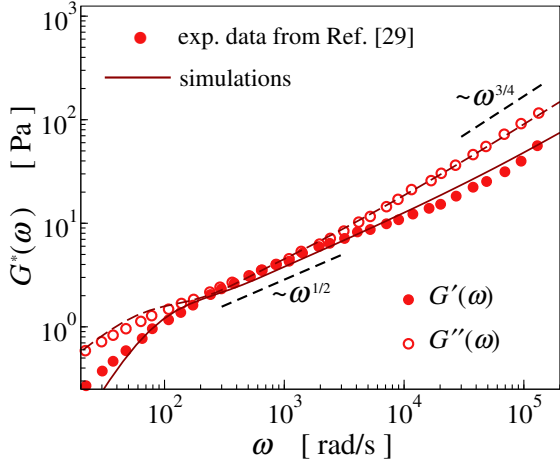


Figure 5: Comparison between the shear moduli obtained from relaxation simulations (continuous lines), as described in Sec. 3.4, and the experimental data (circles) obtained for DNA solutions [29]. Relaxation simulations were performed for long chains with $N = 1000$ beads using PBC and an external force $F_0 = 1$ pN, $\Delta t = 10^{-6}$ μ s, $D_0 = 2.57$ nm²/ μ s, $k_B T = 4.086$ pN.nm ($T = 296$ K), $b = 0.99$ nm, $\kappa = 12.426$ pN/nm, $\kappa_b = 2098.7$ pN/nm, so that $A = 498$ nm, $\tau_f = 0.013$ s, and $\eta_0 = 0.03$ Pa.s. The number density of DNA molecules in solution is estimated as $n_f \approx 43 \times 10^{13}$ cm⁻³.

and the relative viscosity is given by $\eta'(\omega)/\eta_0 \propto \omega^{\alpha-1}$, with a characteristic exponent $\alpha \approx 3/4$, in agreement to previous theoretical and computational studies presented in the literature [17, 25, 26, 30, 31, 32]. Also, as expected from the dynamics, one can verify from the inset of Figs. 4(c) and 4(d) that the low frequency regime of the reduced moduli and the relative viscosity is not altered due to the introduction of the bending energy.

A careful look at Fig. 4(c) indicates that, in addition to the power-law behaviour observed for the shear moduli with a somewhat characteristic exponent $\alpha = 3/4$, the rheology of solutions of semiflexible filaments might display intermediary values for α , also including a transition regime from the flexible behaviour with exponent $\alpha = 1/2$. In order to illustrate that idea we include comparisons between the numerical results obtained from our relaxation simulations and experimental data extracted from microrheology experiments.

For instance, Fig. 5 shows the viscoelastic response obtained for a diluted solution of DNA [29], which is very similar to the behaviour observed for intermediary values of A and long filaments showed in Fig. 4(c), that is, a transition from a subdiffusive regime with $\alpha \approx 1/2$ at intermediary frequencies to a regime where $G'(\omega) \sim G''(\omega) \sim \omega^{3/4}$, at high frequencies. By considering a number density equal to $n_f \approx 43 \times 10^{13}$ cm⁻³ in Eq. (28), we were able to observe a good quantitative

agreement between the numerical results and the experimental data, indicating the effectiveness of our approach, despite of the fact that we have used a simple bead-spring model to perform the relaxation simulations.

Finally, we include in Fig. 6 a comparison between the numerical results obtained from our relaxation simulations and the experimental data on solutions of collagen at 2 mg/mL extracted from Ref. [36]. Interestingly, the exponent α observed for the power-law behaviour of the shear moduli in Fig. 6(a) present a value between $1/2$ and $3/4$ at an intermediary frequency range. The value of $\alpha \approx 0.7$ is corroborated by the behaviour of the viscosity $\eta'(\omega) \propto \omega^{\alpha-1}$, which is displayed in Fig. 6(b). As discussed in Ref. [36], such intermediary behaviour between flexible and semiflexible could be explained due to ratio between the short contour length ($L \approx 300$ nm) and the persistent length of the collagen molecules ($L_p \approx 15 - 160$ nm), which put the viscoelastic response of the corresponding solution in a crossover region. Although the experimental data of Ref. [36] do not include the low frequency regime of the viscoelastic functions, we estimate the number of segments from $\eta'(\omega)$, just as discussed at the end of Sec. 3.4. Importantly, the quantitative agreement between our numerical results and the experimental data presented in Fig. 6 indicate that the relaxation simulations can be also applied to obtain the viscoelastic response of solutions with shorter filaments, as in the case of collagen [36].

5. Concluding remarks

In this work we present an efficient numerical method based on relaxation simulations that allow one to evaluate the full viscoelastic response of both flexible and semiflexible filament solutions. By considering the universal character of the microrheology of complex solutions at the low frequency regime, we have derived useful relations that allowed us to obtain the shear moduli and the viscosity of unentangled filament solutions without having to resort to shearing protocols that are commonly used for solutions with cross-linked and tightly entangled filaments.

It is worth mentioning that, since the theoretical basis of our relaxation simulations is the fluctuation-dissipation theorem, the determination of the mean-squared displacement and the time-dependent diffusion coefficient of the beads through Eqs. (22) and (23), respectively, does not need to be based on brownian dynamics simulations to be accomplished. In fact, we expect that one can explore those equations together with, for example, usual molecular dynamics simulations.

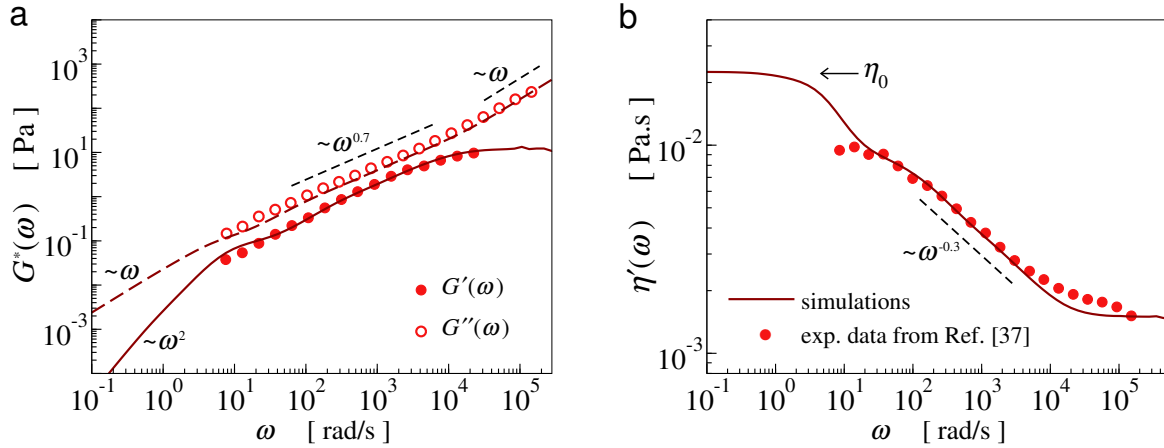


Figure 6: Comparison between the viscoelastic properties obtained from relaxation simulations (lines), as described in Sec. 3.4, and the experimental data (circles) extracted from Ref. [36], which corresponds to solutions of collagen at 2 mg/mL. (a) storage modulus (filled circles), $G'(\omega)$, and loss modulus (open circles), $G''(\omega)$; and (b) the viscosity $\eta'(\omega) = G''(\omega)/\omega$. Relaxation simulations were performed for short chains with $N = 15$ beads using FBC with an external force $F_0 = 1$ pN, $\Delta t = 1$ ns, $D_0 = 7.28$ nm²/s, $k_B T = 4.059$ pN.nm ($T = 294$ K), $b = 0.99$ nm, $\kappa = 12.42$ pN/nm, $\kappa_b = 699$ pN/nm, so that $A = 167$ nm, $\tau_f \approx 1.02$ s, and $\eta_0 = 0.0224$ Pa.s. The number density of collagen molecules in solution is estimated as $n_f \approx 0.4 \times 10^{13}$ cm⁻³.

Finally, we note that the good agreement to experimental data achieved by the numerical results obtained from our relaxation simulations should encourage the use of such numerical methodology combined with more detailed filament models (*e.g.*, [37, 38]). In particular, one can extend the relaxation simulations to include hydrodynamic interactions and excluded volume effects [25]. Also, it should be worthwhile to apply the relaxation simulations in the characterization of the viscoelastic response of solutions of intrinsically disordered proteins (see, *e.g.*, [39]), which are heteropolymers that present different flexibility along the chain.

Acknowledgements

L. G. Rizzi acknowledges the financial support of the Brazilian agencies CNPq (Grants N^o 306302/2018-7 and N^o 426570/2018-9) and FAPEMIG (Process APQ-02783-18), although no funding was released until the submission of the present work; L. K. R. Duarte thanks the scholarship from the Brazilian agency CAPES.

References

- [1] L. G. Rizzi, M. Tassieri, Microrheology of biological specimens, *Encyclopedia of Analytical Chemistry* (2018).
- [2] R. H. Pritchard, Y. Y. S. Huang, E. M. Terentjev, Mechanics of biological networks: from the cell cytoskeleton to connective tissue, *Soft Matter*, 10 (2014) 1864.

- [3] C. Lang, J. Hendricks, Z. Zhang, N. K. Reddy, J. P. Rothstein, M. P. Lettinga, J. Vermant, C. Clasen, Effects of particle stiffness on the extensional rheology of model rod-like nanoparticle suspensions, *Soft Matter* 15 (2019) 833.
- [4] C. Broedersz, F. MacKintosh, Modeling semiflexible polymer networks, *Rev. Mod. Phys.* 86 (2014) 995.
- [5] L. G. Rizzi, D. A. Head, S. Auer, Universality in the morphology and mechanics of coarsening amyloid fibril networks, *Phys. Rev. Lett.* 114 (2015) 078102.
- [6] L. G. Rizzi, S. Auer, D. A. Head, Importance of non-affine viscoelastic response in disordered fibre networks, *Soft Matter* 12 (2016) 4332.
- [7] F. Meng, E. M. Terentjev, Theory of semiflexible filaments and networks, *Polymers* 9 (2017) 52.
- [8] C. Cruz, F. Chinesta, G. Régner, Review on the brownian dynamics simulation of bead-rod-spring models encountered in computational rheology, *Arch. Comput. Methods Eng.* 19 (2012) 227.
- [9] F. Gittes, B. Schnurr, P. D. Olmsted, F. C. MacKintosh, C. F. Schmidt, Microscopic viscoelasticity: Shear moduli of soft materials determined from thermal fluctuations, *Phys. Rev. Lett.* 79 (1997) 3286.
- [10] M. Tassieri, T. A. Waigh, J. Trinick, A. Aggeli, R. M. L. Evans, Analysis of the linear viscoelasticity of polyelectrolytes by magnetic microrheometry - Pulsed creep experiments and the one particle response, *J. Rheol.* 54 (2010) 117.
- [11] D. A. Head, E. Ikebe, A. Nakamasu, P. Zhang, L. G. Villaruz, S. Kinoshita, S. Ando, D. Mizuno, High-frequency affine mechanics and nonaffine relaxation in a model cytoskeleton, *Phys. Rev. E* 89 (2014) 042711.
- [12] P. Licinio, A. V. Teixeira, Anomalous diffusion of ideal polymer networks, *Phys. Rev. E* 56 (1997) 631.
- [13] P. Licinio, A. V. Teixeira, Relaxation of ideal polymer networks, *Philos. Mag. B* 78 (1998) 171.
- [14] A. V. Teixeira, P. Licinio, Dynamics of swollen fractal networks, *Europhys. Lett.* 45 (1999) 162.
- [15] R. G. Larson, *The Structure and Rheology of Complex Fluids*, Oxford University Press, 1999.

- [16] J. D. Ferry, Viscoelastic properties of polymers, 3rd Edition, John Wiley & Sons, 1980.
- [17] M. Rubinstein, R. H. Colby, Polymer Physics, Oxford University Press, 2003.
- [18] M. Doi, Soft Matter Physics, Oxford University Press, 2013.
- [19] S.-P. Li, G. Zhao, H.-Y. Chen, The relationship between steady shear viscosity and complex viscosity, J. Disper. Sci. Technol. 26 (2005) 415.
- [20] T. M. Squires, T. G. Mason, Fluid mechanics of microrheology, Annu. Rev. Fluid Mech. 42 (2010) 413.
- [21] T. A. Waigh, Advances in the microrheology of complex fluids, Rep. Prog. Phys. 79 (2016) 074601.
- [22] M. Tassieri, F. D. Giudice, E. Robertson, N. Jain, B. Fries, R. Wilson, A. Glidle, F. Greco, P. A. Netti, P. L. Maffettone, T. Bicanic, J. M. Cooper, Microrheology with optical tweezers: Measuring the relative viscosity of solutions ‘at a glance’, Sci. Rep. 5 (2015) 8831.
- [23] T. G. Mason, Estimating the viscoelastic moduli of complex fluids using the generalized stokes-einstein equation, Rheol. Acta 39 (2000) 371.
- [24] M. Doi, S. F. Edwards, The Theory of Polymer Dynamics, Oxford University Press, 1986.
- [25] A. Nikoubashman, A. Milchev, K. Binder, Dynamics of single semiflexible polymers in dilute solution, J. Chem. Phys. 145 (2016) 234903.
- [26] V. Shankar, M. Pasquali, D. C. Morse, Theory of linear viscoelasticity of semiflexible rods in dilute solution, J. Rheol. 46 (2002) 1111.
- [27] M. Tassieri, R. M. L. Evans, R. L. Warren, N. J. Bailey, J. M. Cooper, Microrheology with optical tweezers: Data analysis, New J. Phys. 14 (2012) 115032.
- [28] E. Sarmiento-Gomez, D. Montalvan-Sorrososa, C. Garza, J. Mas-Oliva, R. Castillo, Rheology and dws microrheology of concentrated suspensions of the semiflexible filamentous fd virus., Eur. Phys. J. E 35 (2012) 35.
- [29] B. A. Krajina, C. Tropini, A. Zhu, P. DiGiacomo, J. L. Sonnenburg, S. C. Heilshorn, A. J. Spakowitz, Dynamic light scattering microrheology reveals multiscale viscoelasticity of polymer gels and precious biological materials, ACS Cent. Sci. 3 (2017) 1294.
- [30] M. Pasquali, V. Shankar, D. C. Morse, Viscoelasticity of dilute solutions of semiflexible polymers, Phys. Rev. E 64 (2001) 020802.
- [31] P. Dimitrakopoulos, J. F. Brady, Z.-G. Wang, Short- and intermediate-time behavior of the linear stress relaxation in semiflexible polymers, Phys. Rev. E 64 (2001) 050803.
- [32] E. F. Koslover, A. J. Spakowitz, Multiscale dynamics of semiflexible polymers from a universal coarse-graining procedure, Phys. Rev. E 90 (2014) 013304.
- [33] A. E. Likhtman, S. K. Sukumaran, J. Ramirez, Linear viscoelasticity from molecular dynamics simulation of entangled polymers, Macromolecules 40 (2007) 6748.
- [34] D. T. Gillespie, Fluctuation and dissipation in brownian motion, Am. J. Phys. 61 (1993) 1077.
- [35] R. M. L. Evans, M. Tassieri, D. Auhl, T. A. Waigh, Direct conversion of rheological compliance measurements into storage and loss moduli, Phys. Rev. E 80 (2009) 012501.
- [36] M. Shayegan, N. R. Forde, Microrheological characterization of collagen systems: From molecular solutions to fibrillar gels, Plos ONE 8 (2013) e70590.
- [37] E. F. Koslover, A. J. Spakowitz, Discretizing elastic chains for coarse-grained polymer models, Soft Matter 9 (2013) 7016.
- [38] R. D. Groot, Mesoscale simulation of semiflexible chains. I. endpoint distribution and chain dynamics, J. Chem. Phys. 138 (2013) 224903.
- [39] R. B. Frigori, L. G. Rizzi, N. A. Alves, Microcanonical thermostatics of coarse-grained proteins with amyloidogenic propensity, J. Chem. Phys. 138 (2013) 015102.